

Change detection in polarimetric SAR images

Synthesis in Earth and Space Physics

DTU

Victor Poughon, s131253

Supervisors: Henning Skriver, Allan Aasbjerg Nielsen

27/02/2015

Abstract

Polarimetric SAR systems are a very popular sensor choice for airborne and satellite platforms, and are very useful for all types of monitoring applications. The problem of change detection is the quantitative characterization of differences between images of the same target acquired at different times. This project presents and investigates different change detection methods using data from the airborne EMISAR system, a fully polarimetric C-band and L-band synthetic aperture radar. After exposing the theory of different likelihood ratio test statistics, the results of their application to the EMISAR data set is presented. Emphasis is put on interpretation and visualization of change detection images.

Table of contents

Abstract	2
1 Introduction	4
2 Theory	5
2.1 Polarimetric SAR	5
2.2 Classical change detection	5
2.3 Wishart distribution test statistic	6
2.4 Special cases	7
2.5 Omnibus test	8
2.6 R_j test	9
3 Data	10
4 Results	12
4.1 Gamma parameter test statistic	12
4.2 Complex Wishart test statistic	20
4.3 Omnibus test statistic	24
4.4 R_j test statistic	27
5 Implementation	33
5.1 Tools	33
5.2 Efficiency considerations	33
6 Conclusion	35

1 Introduction

Radar systems are a popular advanced data acquisition system. The availability of polarimetric SAR data from both satellite and aerial platforms have made it a great choice for many monitoring applications.

The focus of this project is the detection of change in polarimetric SAR images. Which methods can quantify the difference between multiple radar images of the same target?

The task is not trivial because of the nature of a radar signal. Contrary to visible light images, the pixels of a radar signal are represented by 3×3 covariance matrices. Specialized methods are therefore needed to effectively quantify change.

This report first exposes the theory behind the possible change detection methods. Each method is based on a likelihood ratio test statistic for testing a null hypothesis H_0 . The distribution of this likelihood ratio is known under the null hypothesis. This is useful for obtaining p-values, a statistically meaningful interpretation of the results. All methods presented are implemented in the Python scientific programming Scipy environment. The analysis is based on data available from the EMISAR system. The time series used contains images of the Foulum region in Denmark for each month from March 1999 to August 1998. The Results section focuses on the different ways of presenting the output of the change detection procedures and how they can be interpreted.

2 Theory

2.1 Polarimetric SAR

Polarimetric SAR measures the amplitude and phase of the incident and scattered signal. The signal is typically represented with four polarizations combinations:

$$\mathbf{S} = \begin{bmatrix} S_{hh} \\ S_{hv} \\ S_{vh} \\ S_{vv} \end{bmatrix} \quad (1)$$

Natural target most often have *reciprocity*, and therefore in most cases $S_{hv} = S_{vh}$. Only a 3-vector is then used:

$$\mathbf{S} = \begin{bmatrix} S_{hh} \\ S_{hv} \\ S_{vv} \end{bmatrix} \quad (2)$$

Spatial averaging is used to reduce noise, and in that case the average covariance matrix is the appropriate representation.

$$\langle \mathbf{C} \rangle = \langle \mathbf{SS}^* \rangle = \begin{bmatrix} \langle S_{hh} S_{hh}^* \rangle & \langle S_{hh} S_{hv}^* \rangle & \langle S_{hh} S_{vv}^* \rangle \\ \langle S_{hv} S_{hh}^* \rangle & \langle S_{hv} S_{hv}^* \rangle & \langle S_{hv} S_{vv}^* \rangle \\ \langle S_{vv} S_{hh}^* \rangle & \langle S_{vv} S_{hv}^* \rangle & \langle S_{vv} S_{vv}^* \rangle \end{bmatrix} \quad (3)$$

where $\langle \cdot \rangle$ is ensemble averaging. The so called equivalent number of looks, or ENL, is the number of independent samples, also related to the size of the spatial averaging area.

2.2 Classical change detection

The problem of change detection is to find and expose differences between two or more images of the same area. The first method investigated here is the classical method. The representation of a single data point (a pixel) is 3-dimensional, but this method simplifies the problem by only considering one channel. It is based on a likelihood ratio test for the equality of two gamma parameters. Let X and Y be independent random variables and gamma distributed

$$\begin{aligned} X &\in G(n, \beta_x) \\ Y &\in G(m, \beta_y) \end{aligned} \quad (4)$$

m and n are the ENL of each observation. X and Y represent observations of the same location at different times. The null hypothesis of this test is that the two parameters are equal:

$$H_0 : \beta_x = \beta_y \quad (5)$$

The likelihood ratio test statistic is then:

$$Q = \frac{Y}{X} \quad (6)$$

More details and the derivation are in [2]. The critical region is

$$\frac{Y}{X} \leq c_1 \text{ or } \frac{Y}{X} \geq c_2 \quad (7)$$

In other words change is detected (H_0 is rejected) when Q is within the critical region. Y/X under the null hypothesis (in a region with no change) is distributed like Fisher's F :

$$\frac{m}{n} \frac{Y}{X} \in F(2m, 2n) \quad (8)$$

Therefore c_1 and c_2 can be determined in a statistically significant manner from the quantiles of the F-distribution.

2.3 Wishart distribution test statistic

A more complete change detection method needs to make use of all three polarization elements. A test statistic for the equality of two complex Wishart distributed covariance matrix was introduced in [2]. Let X and Y now be the covariance matrices of two data points at different times. They are of size $p = 3$ and complex Wishart distributed:

$$\begin{aligned} \mathbf{X} &\in W_c(p, n, \Sigma_x) \\ \mathbf{Y} &\in W_c(p, m, \Sigma_y) \end{aligned} \quad (9)$$

Similarly, the null hypothesis is equality of the two Σ parameters:

$$H_0 : \Sigma_x = \Sigma_y \quad (10)$$

In this case the likelihood test statistic becomes

$$Q = \frac{(n+m)^{p(n+m)}}{n^{pn} m^{pm}} \frac{|\mathbf{X}|^n |\mathbf{Y}|^m}{|\mathbf{X} + \mathbf{Y}|^{n+m}} \quad (11)$$

n and m are the ENL of each observation and might be different. In logarithmic form:

$$\ln Q = p(n+m) \ln(n+m) - pn \ln(n) - pm \ln(m) + n \ln |\mathbf{X}| + m \ln |\mathbf{Y}| - (n+m) \ln |\mathbf{X} + \mathbf{Y}| \quad (12)$$

The theoretical distribution of this test statistic is approximated by

$$P\{-2\rho \ln Q \leq z\} \approx P\{\chi^2(p^2) \leq z\} + \omega_2 \left[P\{\chi^2(p^2 + 4) \leq z\} - P\{\chi^2(p^2) \leq z\} \right] \quad (13)$$

where

$$\begin{aligned} \rho &= 1 - \frac{2p^2 - 1}{6p} \left(\frac{1}{n} + \frac{1}{m} - \frac{1}{n+m} \right) \\ \omega_2 &= -\frac{p^2}{4} \left(1 - \frac{1}{\rho} \right)^2 + \frac{p^2(p^2 - 1)}{24} \cdot \left(\frac{1}{n^2} + \frac{1}{m^2} - \frac{1}{(n+m)^2} \right) \frac{1}{\rho^2} \end{aligned} \quad (14)$$

2.4 Special cases

The test statistic based on the complex Wishart distribution uses the full covariance matrix C . In the interest of better computational speed, simplified calculations or simpler radar systems, it is possible to consider reduced cases.

2.4.1 Block diagonal

In the block diagonal case, only the diagonal elements of C are used. The determinant is reduced to the product of the three real diagonal elements.

$$\langle \mathbf{C} \rangle = \begin{bmatrix} \langle S_{hh}S_{hh}^* \rangle & 0 & 0 \\ 0 & \langle S_{hv}S_{hv}^* \rangle & 0 \\ 0 & 0 & \langle S_{vv}S_{vv}^* \rangle \end{bmatrix} \quad (15)$$

2.4.2 Azimuthal symmetry

In the azimuthal symmetric case

$$\begin{bmatrix} \langle S_{hh}S_{hh}^* \rangle & \langle S_{hh}S_{vv}^* \rangle & 0 \\ \langle S_{vv}S_{hh}^* \rangle & \langle S_{vv}S_{vv}^* \rangle & 0 \\ 0 & 0 & \langle S_{hv}S_{hv}^* \rangle \end{bmatrix} = \begin{bmatrix} \mathbf{X}_1 & 0 \\ 0 & \mathbf{X}_2 \end{bmatrix} \quad (16)$$

2.5 Omnibus test

The previous methods are limited to detecting change between two points in time. In many cases a complete time series of data is available. One could simply perform pairwise comparisons over each successive pair, but this approach has some drawbacks. It is then natural to design a change detection method adapted to many points in time.

This however raises the question of which hypothesis is to be tested? There are several possibilities regarding the presence of change in a time series of more than two elements. How much change is there? When does it occur? Does it have any regular structure?

The Omnibus test [1] is designed to test the hypothesis of the presence of any change in the time series. In other words, H_0 is now

$$\Sigma_1 = \Sigma_2 = \dots = \Sigma_k \quad (17)$$

Where, following earlier assumptions, the Σ_k are the parameters of complex Wishart distributed covariance matrices.

$$\mathbf{X}_i \in W_c(p, n, \Sigma_i) \quad (18)$$

In an image each X_i represents the same pixel at different times.

The test statistic for this hypothesis is:

$$Q = \left\{ k^{pk} \frac{\prod_{i=1}^k |\mathbf{X}_i|}{|\mathbf{X}|^k} \right\}^n \quad (19)$$

where $\mathbf{X} = \sum_{i=1}^k \mathbf{X}_i$ and n as usual is the equivalent number of looks. Or in logarithm form:

$$\ln Q = n \left\{ pk \ln k + \sum_{i=1}^k \ln |\mathbf{X}_i| - k \ln |\mathbf{X}| \right\} \quad (20)$$

The distribution of this test is such that finding a smaller value of $-2\rho \ln Q$ is:

$$P\{-2\rho \ln Q \leq z\} \approx P\{\chi^2(f) \leq z\} + \omega_2 \left[P\{\chi^2(f+4) \leq z\} - P\{\chi^2(f) \leq z\} \right] \quad (21)$$

where

$$\begin{aligned} f &= (k-1)p^2 \\ \rho &= 1 - \frac{2p^2 - 1}{6(k-1)p} \left(\frac{k}{n} - \frac{1}{nk} \right) \\ \omega_2 &= \frac{p^2(p^2-1)}{24\rho^2} \left(\frac{k}{n^2} - \frac{1}{(nk)^2} \right) - \frac{p^2(k-1)}{4} \left(1 - \frac{1}{\rho} \right)^2 \end{aligned} \quad (22)$$

2.6 R_j test

The result of the previous Omnibus test is binary. Either H_0 is refuted, and change is detected, or it isn't. If the presence of some change is indicated in the time series, the next natural question is to ask: when does change occur? This is the purpose of the R_j test statistic, introduced in [3]. More specifically, it is a test for the equality of the first $j < k$ covariance matrices. Used successively from $j = 2$ to $j = k$, this allows finding the exact time points where change occurs.

Given that there is no change within the first k elements of the series, i.e. :

$$\Sigma_1 = \Sigma_2 = \dots = \Sigma_{j-1} \quad (23)$$

the hypothesis tested is:

$$H_{0,j} : H_j = H_{j-1} \quad (24)$$

with the likelihood ratio test statistic R_j :

$$R_j = \left\{ \frac{j^{jp}}{(j-1)^{(j-1)p}} \frac{|\mathbf{X}_1 + \dots + \mathbf{X}_{j-1}|^{(j-1)} |\mathbf{X}_j|}{|\mathbf{X}_1 + \dots + \mathbf{X}_j|^j} \right\}^n \quad (25)$$

or in logarithmic form:

$$\begin{aligned} \ln R_j = & n \{ p(j \ln j - (j-1) \ln(j-1)) \\ & + (j-1) \ln \left| \sum_{i=1}^{j-1} \mathbf{X}_i \right| + \ln |\mathbf{X}_j| - j \ln \left| \sum_{i=1}^j \mathbf{X}_i \right| \} \end{aligned} \quad (26)$$

Similarly to the other test statistics, interpretation of the result is quantified using the known distribution of $-2\rho_j \ln R_j$:

$$P\{-2\rho_j \ln R_j \leq z\} \approx P\{\chi^2(f) \leq z\} + \omega_2 \left[P\{\chi^2(f+4) \leq z\} - P\{\chi^2(f) \leq z\} \right] \quad (27)$$

where

$$\begin{aligned} f &= p^2 \\ \rho_j &= 1 - \frac{2p^2 - 1}{6pn} \left(1 + \frac{1}{j(j-1)} \right) \\ \omega_{2,j} &= -\frac{p^2}{4} \left(1 - \frac{1}{\rho_j} \right)^2 + \frac{1}{24n^2} p^2 (p^2 - 1) \left(1 + \frac{2j-1}{j^2(j-1)^2} \right) \frac{1}{\rho_j^2} \end{aligned} \quad (28)$$

Equation (27) yields p-values. Deciding upon a fixed significance level is necessary to accept or reject the different hypotheses of equality $H_{0,j}$. Then, repeating the test for all possible periods in the time series yields a table of p-values indicating the likelihood of change at each time point.

3 Data

The data set used in this work is from the EMISAR system, a fully polarimetric synthetic aperture radar. It operates at dual frequencies: C-band (5.3-GHz/5.7-cm) and L-band (1.25-GHz/24-cm). The imaged area is located in Center Foulum in Jutland, Denmark. Agricultural fields are a great test case for polarimetric SAR because scattered signals are very dependent on soil and crop constitution. Agricultural fields also exhibit large seasonal changes which is a perfect application for change detection.

A time series of six images is available with one image for every month from March 1998 to August 1998. Figure 1 is a color composite of the horizontal, vertical and cross polarizations of the image acquired in April. The horizontal and vertical channels are stretched linearly between -30 dB and 0 dB. The cross polarized channel is stretched between -36 dB and -6 dB. Figure 2 is the same color composite, with number indicating the fields as described in the table below.

Labels	Crop
1, 8, 12, 23	Rye
2, 4, 10, 16, 26	Grass
3, 5, 11, 20, 22, 27, 33, 35	Winter Wheat
6, 13, 14, 29, 31, 34, 36	Spring barley
7, 15, 18, 19, 21, 24, 28, 37	Peas
9	Spring oats
17, 25	Winter barley
30	Beets



Figure 1. Color composite image, April 17th 1998.

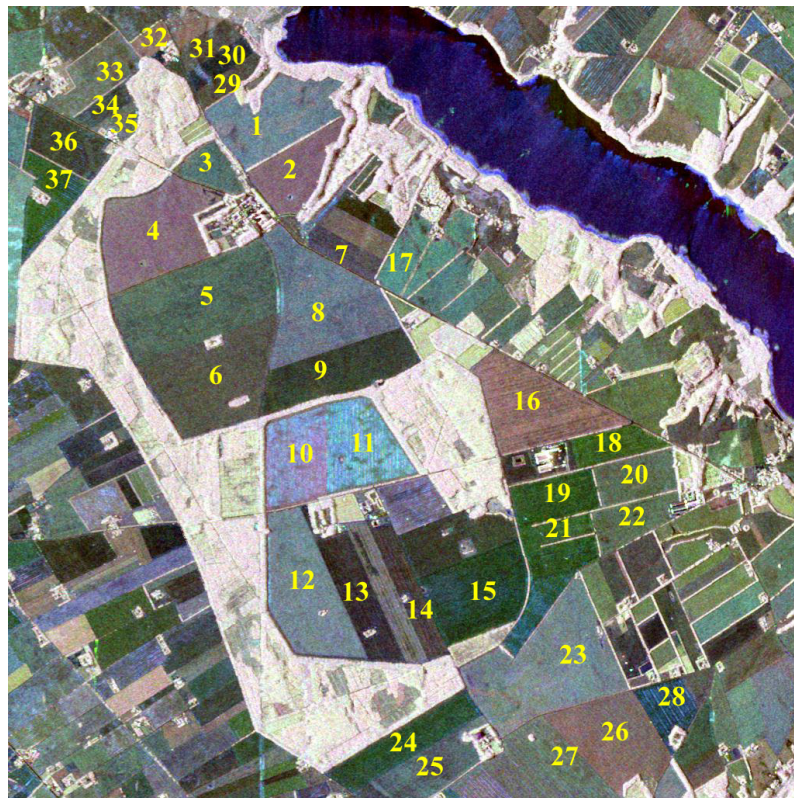


Figure 2. Color composite image, May 20th 1998 with labeled fields.

4 Results

Following the theory section, the general procedure for implementing change detection is to compute a test statistic, select a significance level and a threshold from a distribution percentiles, and apply this threshold over the entire image area to obtain an image. The experimental distribution of a test statistic over a region with no evident change can also be useful as a verification step.

4.1 Gamma parameter test statistic

4.1.1 Images

A simple way to visualize change is a black-and-white image, where white pixels indicate a significant change and black pixels indicate no change. Thresholds based on the critical region defined by equation 7 allow such an implementation where the level of change has a fixed significance level. The F distribution is two-tailed, therefore for a given significance level L , c_1 will be its lower $L/2$ quantile and c_2 its $(1 - L/2)$ quantile. As illustrated in Figure 3, the value of the image $f(x, y)$ is set such that:

$$f(x, y) = \begin{cases} \text{white if } Q \leq c_1 \text{ or } Q \geq c_2 \\ \text{black otherwise} \end{cases}$$

Figures 4, 5 and 6 show the result of this procedure at different significance levels. It is interesting to notice that the results vary when using different polarization elements. For example, the vertical-vertical polarization reveals a high level of change on the edges of the lake, while this is not present in the HV or HH polarizations. The change detection capability is therefore dependent on the polarization considered. This is an inconvenient of the classical method. It uses only a single polarimetric channel which raises some limitations. Only part of the available information is used for detecting change and the result is different based on which channel is used.

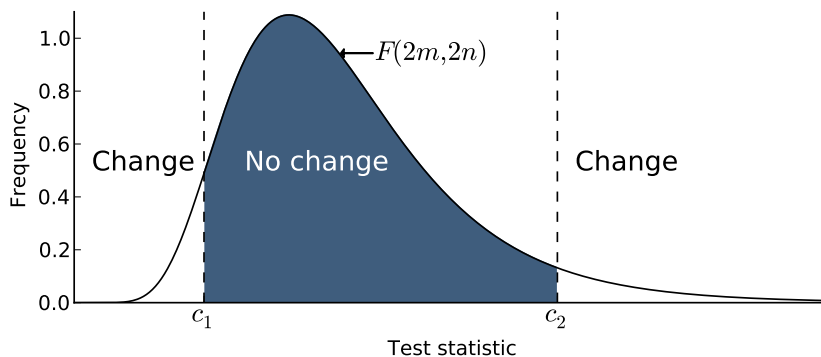


Figure 3. Critical region with the Gamma parameter test statistic.

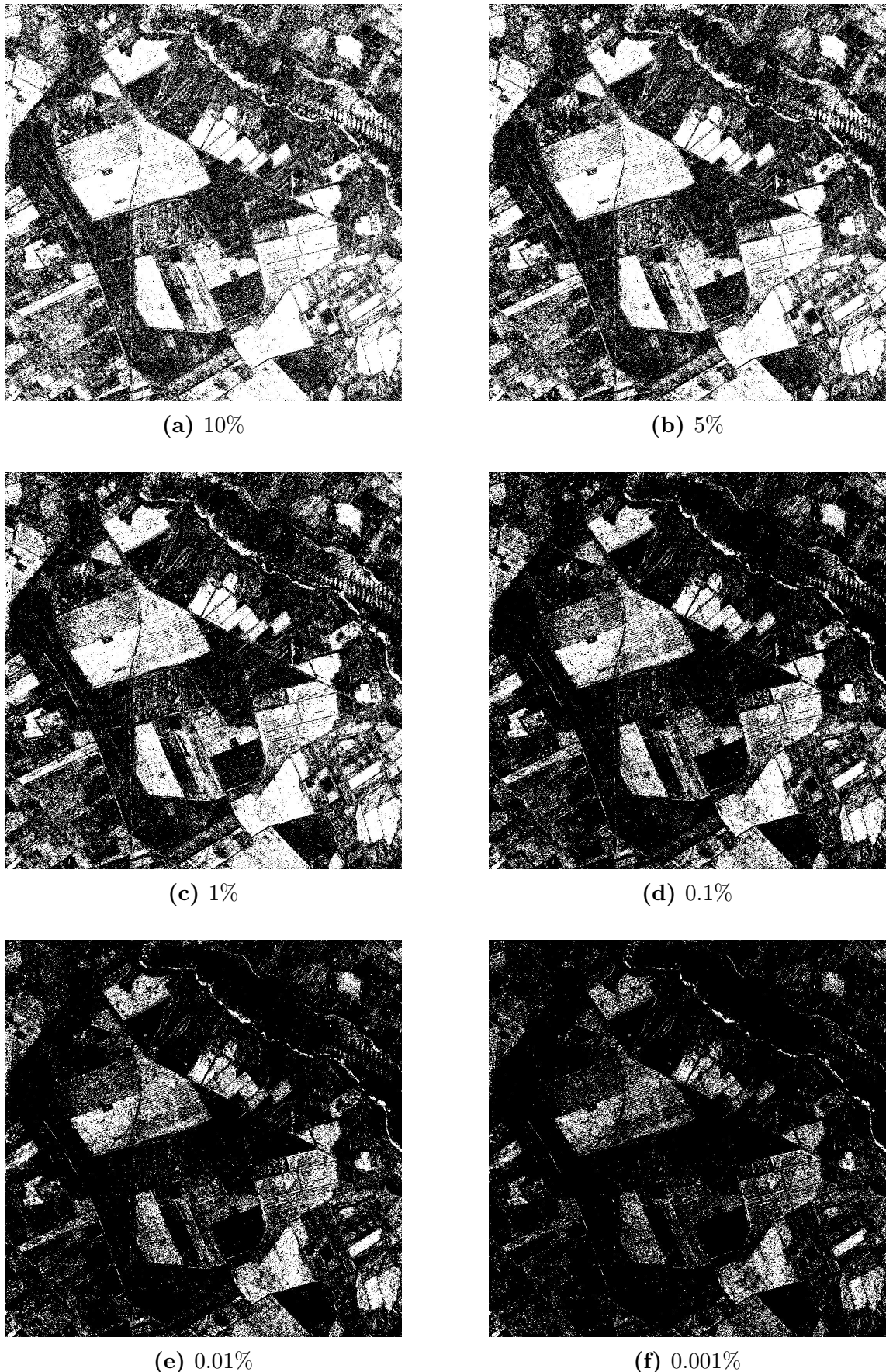


Figure 4. Change detection at different significance levels using the likelihood ratio test statistic Y/X , from the HH polarization channel.

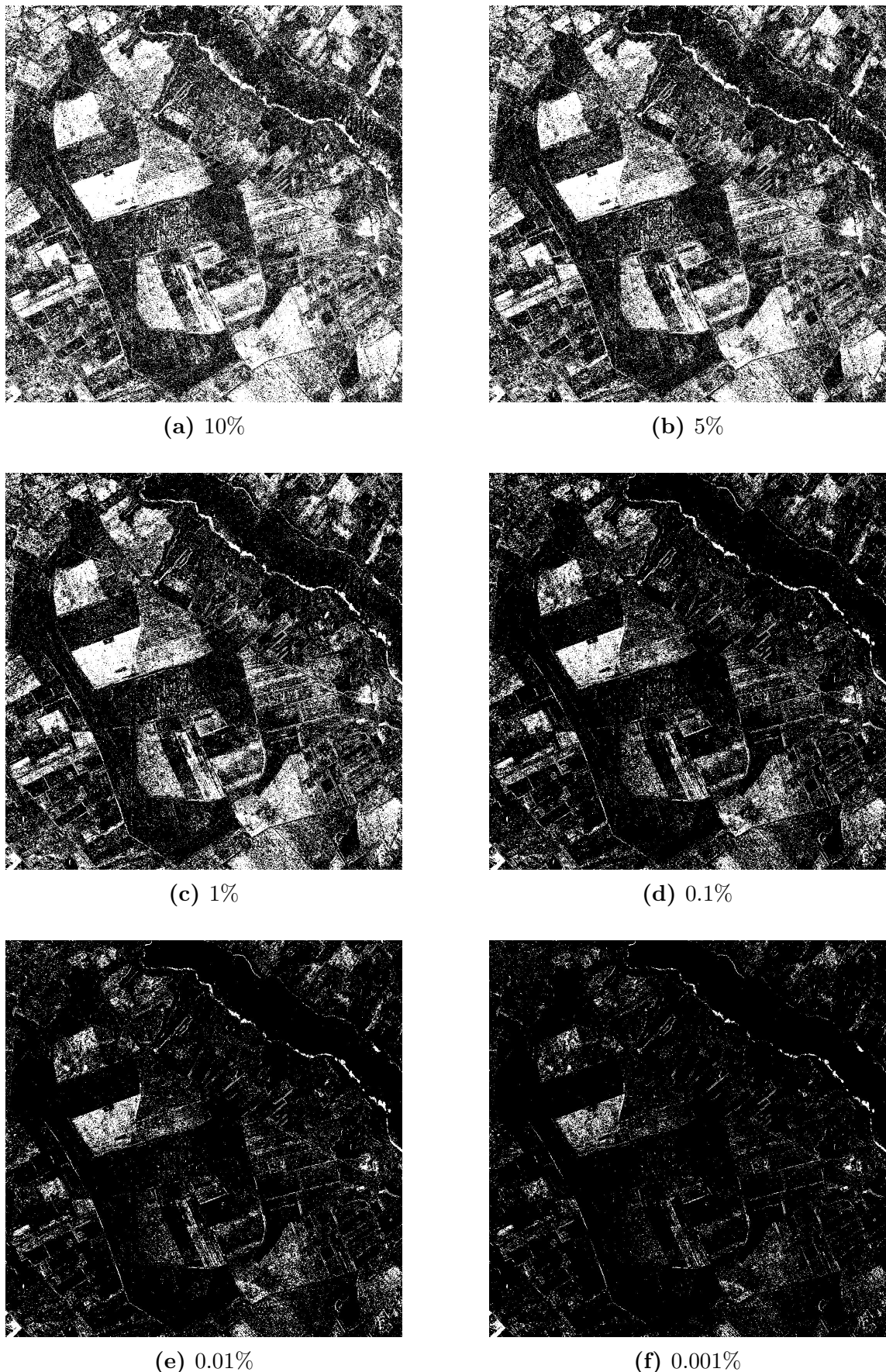


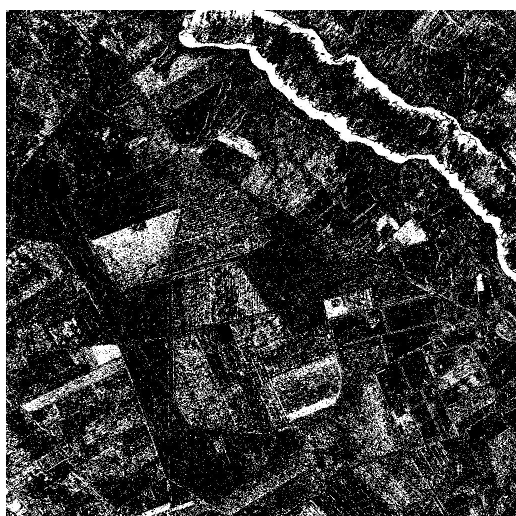
Figure 5. Change detection at different significance levels using the likelihood ratio test statistic Y/X , from the HV polarization channel.



(a) 10%



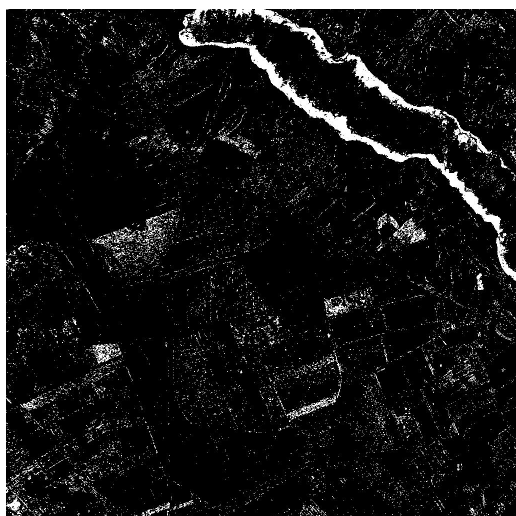
(b) 5%



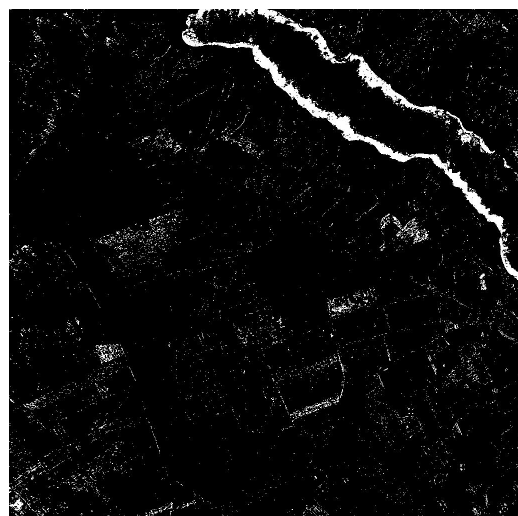
(c) 1%



(d) 0.1%

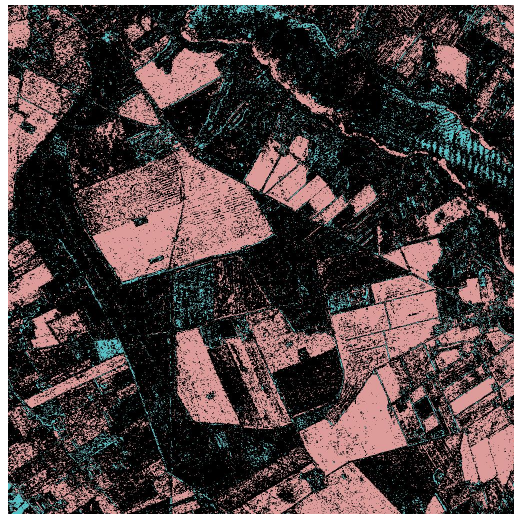


(e) 0.01%

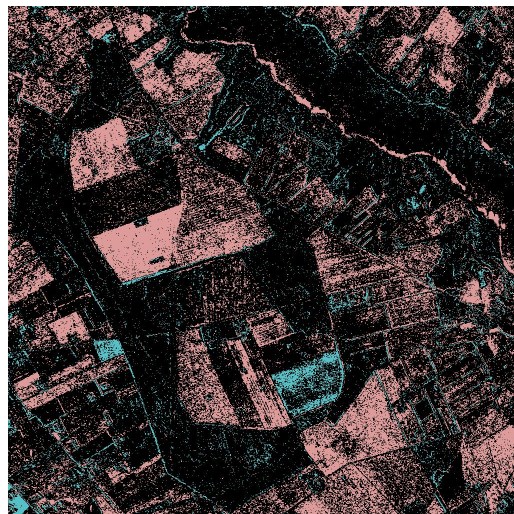


(f) 0.001%

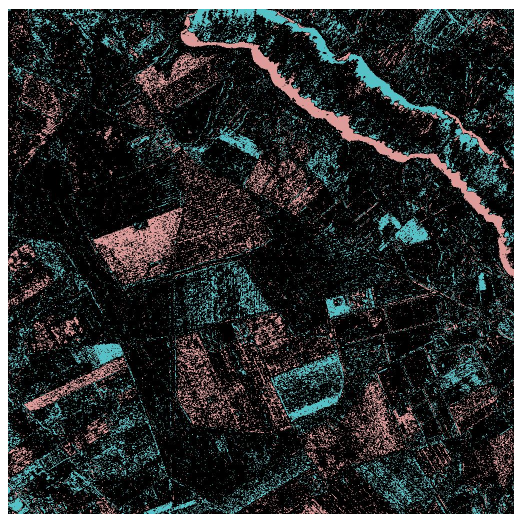
Figure 6. Change detection at different significance levels using the likelihood ratio test statistic Y/X , from the VV polarization channel.



(a) HH channel at 1%.



(b) HV channel at 1%.



(c) VV channel at 1%.

Figure 7. Change detection at 1% significance level using the likelihood ratio test statistic Y/X . Red and green indicate the two tails of the critical region.

4.1.2 No change region

A no change region is selected in the forest area (coniferous). It has very little visible changes in between April and May, It is under the null hypothesis, therefore the gamma parameter test statistic should follow Fisher's F distribution (see (8)) i.e.:

$$\frac{m}{n} \frac{Y}{X} \in F(2m, 2n)$$

Figures 8, 9 and 10 show histograms of the test statistic over the no change region, together with the theoretical probability distribution function for the HH, HV and VV polarization channels.

For all three channels, the probability density function curves are a good fit to the distribution of the test statistic. This is a good confirmation of the theory and also the quality of the data preparation in terms of calibration and processing.

The data was produced with a spatial averaging such that the Equivalent Number of Looks (ENL) is 13. However this is an approximation because the pixels in the image area can be correlated. To investigate the effect of an imprecise ENL, figures 11, 12 and 13 were produced. Different ENL values are tried and the fit of the theoretical distribution can be used for evaluating the number of looks. It appears that $n = m = 13$ is indeed the correct number of looks, and that the test statistic is more sensitive to lower ENL values.

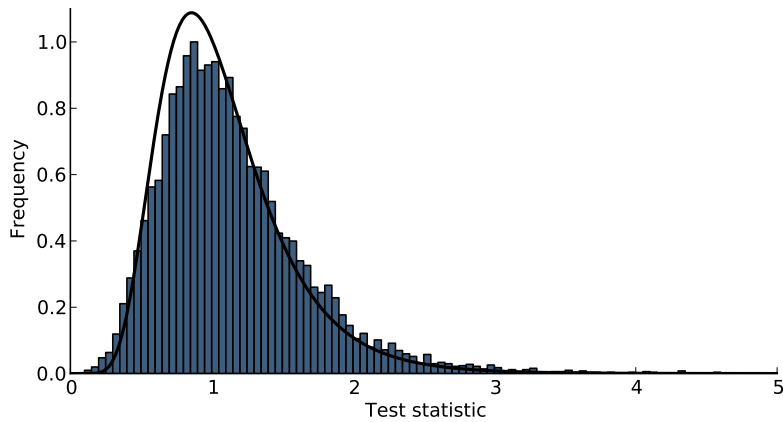


Figure 8. Histogram of Y/X in the no change region, and theoretical pdf, HH channel

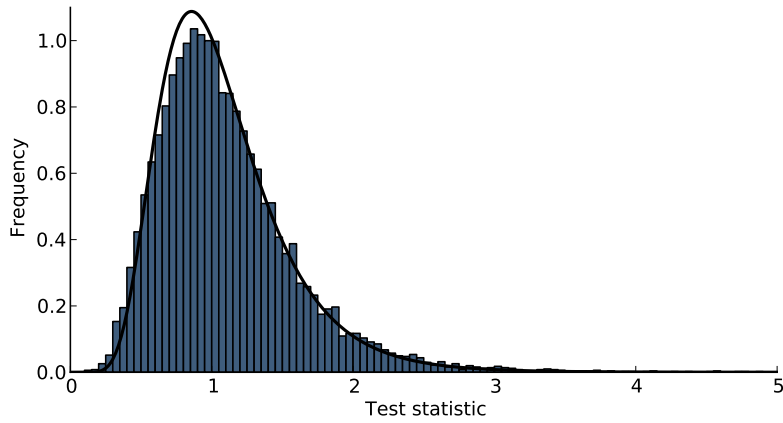


Figure 9. Histogram of Y/X in the no change region, and theoretical pdf, HV channel

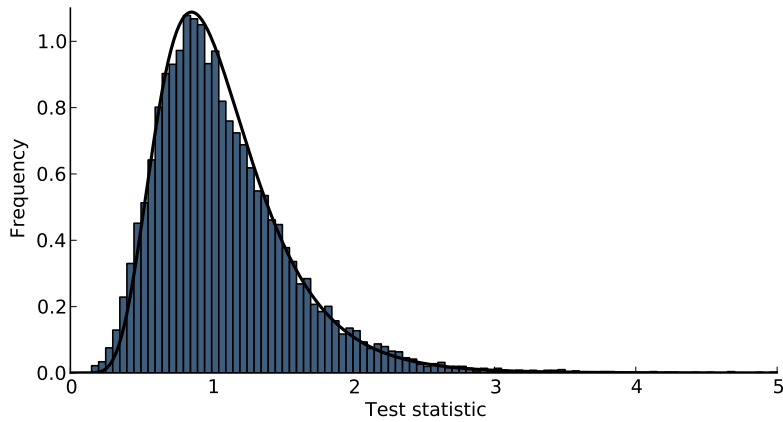


Figure 10. Histogram of Y/X in the no change region, and theoretical pdf, VV channel

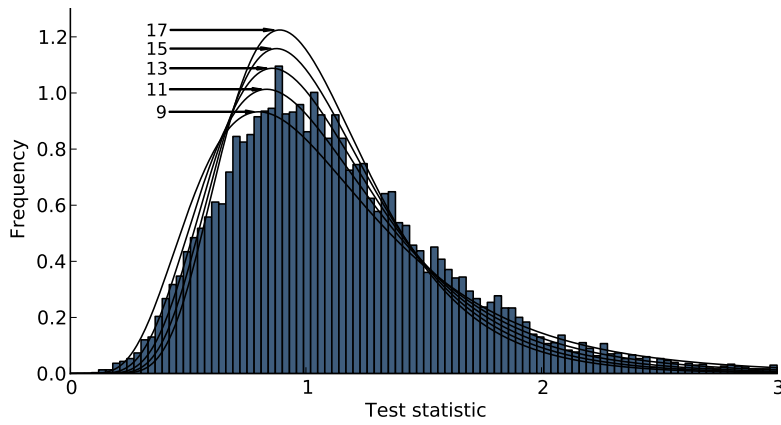


Figure 11. Histogram of Y/X for the HH channel and theoretical PDF for different number of looks.

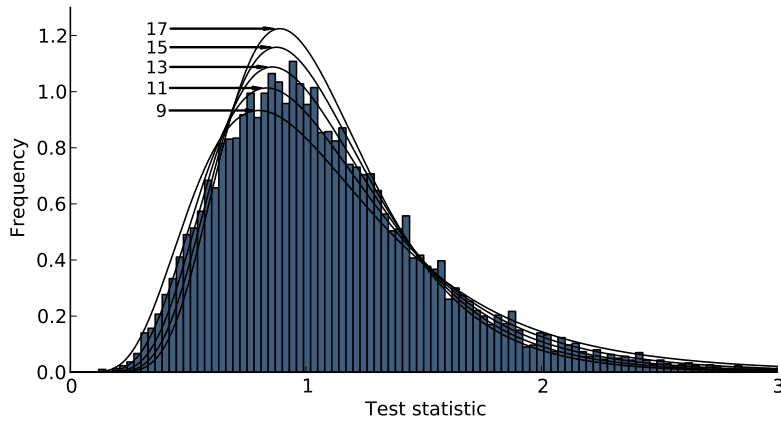


Figure 12. Histogram of Y/X for the HV channel and theoretical PDF for different number of looks.

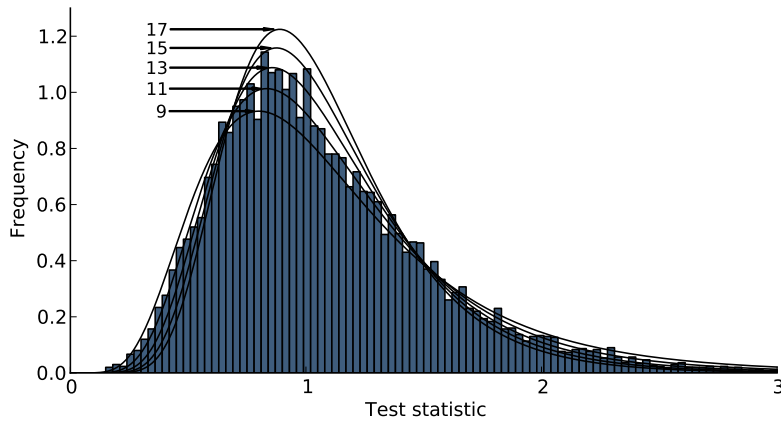


Figure 13. Histogram of Y/X for the VV channel and theoretical PDF for different number of looks.

4.2 Complex Wishart test statistic

This section implements a similar analysis based on equation (11). The test statistic is now computed using all three polarization channels:

$$Q = \frac{(n+m)^{p(n+m)}}{n^{pn}m^{pm}} \frac{|\mathbf{X}|^n |\mathbf{Y}|^m}{|\mathbf{X} + \mathbf{Y}|^{n+m}}$$

where \mathbf{X} and \mathbf{Y} are the complex Wishart distributed covariance matrices at the two time points. Then, a single image can be produced which uses information from all three HH, HV and VV channels.

4.2.1 Images

To produce change detection images with rigorously defined significance levels the quantiles of the distribution defined by equation (13) are needed. However for high ENL values, the ρ and ω_2 terms are can be approximated by 1 and 0, respectively. The approximation used for obtaining quantiles is then:

$$P\{-2 \ln Q \leq z\} \approx P\{\chi^2(p^2) \leq z\} \quad (29)$$

Having selected a threshold T from the quantiles of the χ^2 distribution, the value of the image $f(x, y)$ is set such that:

$$f(x, y) = \begin{cases} \text{white if } -2 \ln Q \geq T \\ \text{black otherwise} \end{cases}$$

This is illustrated in figure 14.

The change detection images produced with this procedure are shown in Figure 17. The main advantage over the Gamma parameter test statistic is that it uses information from all three polarization channels. For example, both the lake and the fields in the middle of the frame are clearly highlighted in a single image. This also entails a simpler interpretation for the user of the change detection system.

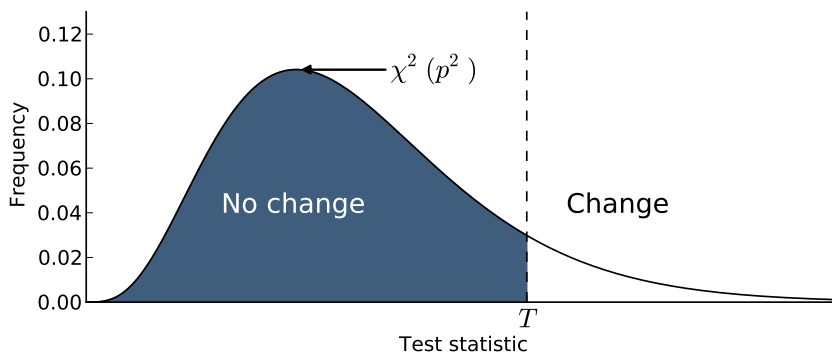


Figure 14. Critical region in the complex Wishart test statistic.

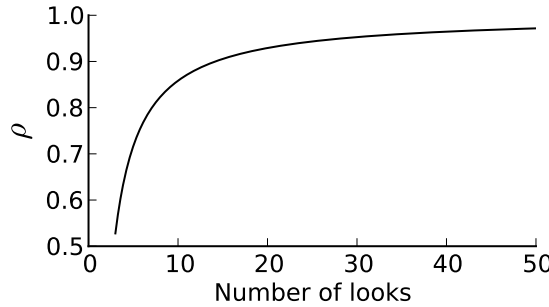


Figure 15. ρ as a function of ENL,
with $n = m$ and $p = 3$.

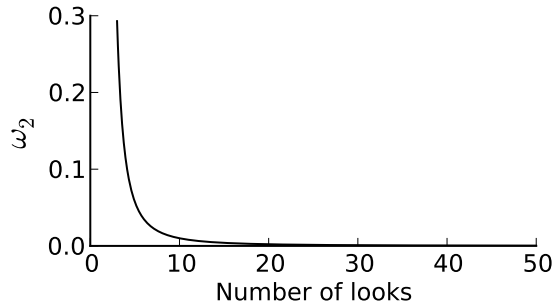


Figure 16. ω_2 as a function of ENL,
with $n = m$ and $p = 3$.

4.2.2 No change region

The no change region is also useful for analysing the Wishart test statistic distribution under the null hypothesis. Figure 18 shows the distribution of $-2 \ln Q$ in the no change region, together with the approximation of its PDF given by equation (29). Visually, the expected and observed distributions are a good match. Similarly to the Gamma parameter test statistic, this underlines the quality of the data and confirms that the assumptions made are reasonable.

Different ENL values have a similar effect, where the test statistic is more sensitive to a number of looks that is too small. This is explained by the ρ and ω_2 terms in equation 14. Figures 15 and 16 show those two parameters as functions of the number of looks. Around $n = m = 13$, ρ and ω_2 are close to 1 and 0, respectively. A poorly estimated ENL will therefore have little effect unless it is close to zero.

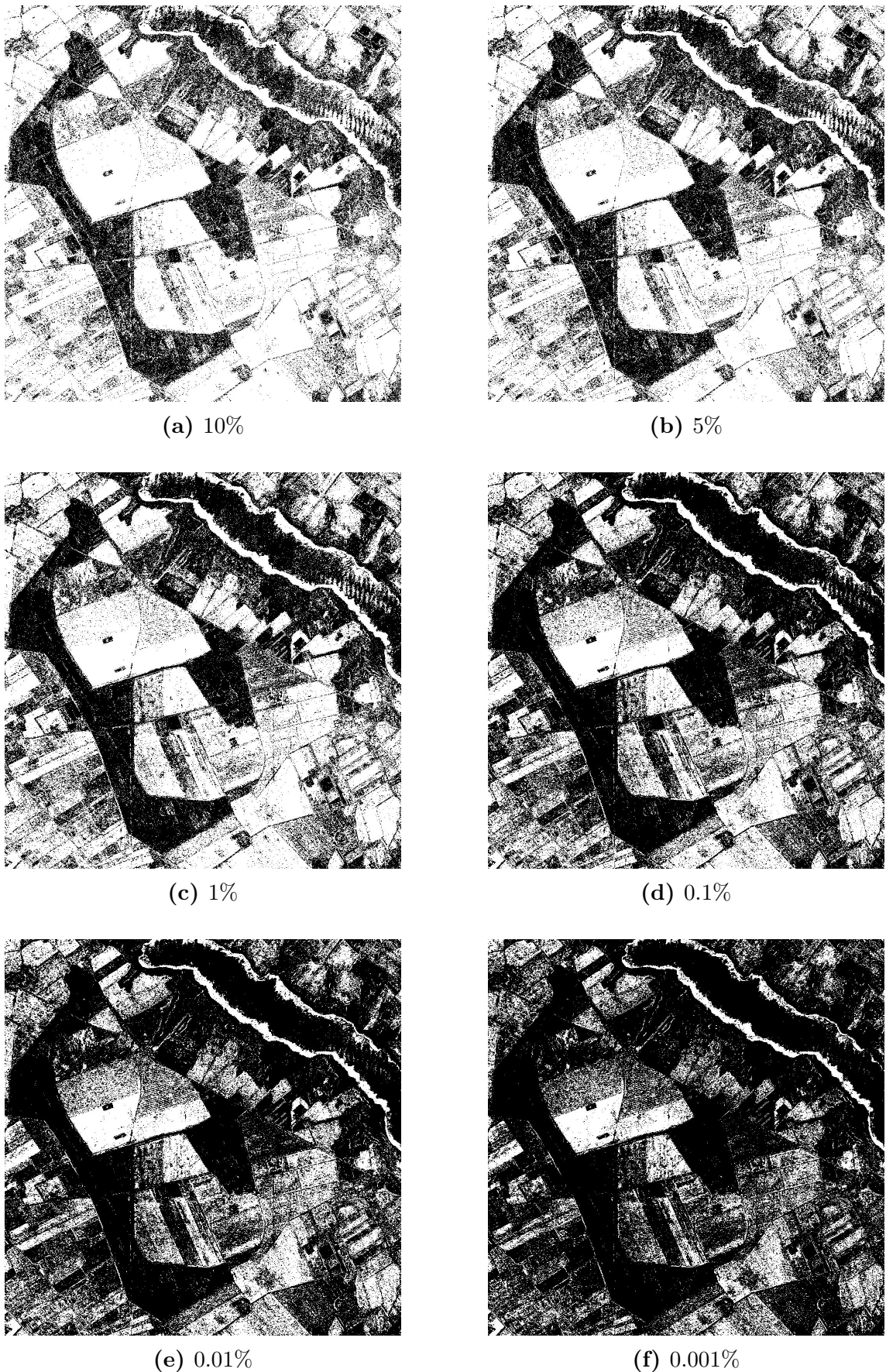


Figure 17. Change detection at different significance levels using the complex Wishart test statistic $-2 \ln Q$.

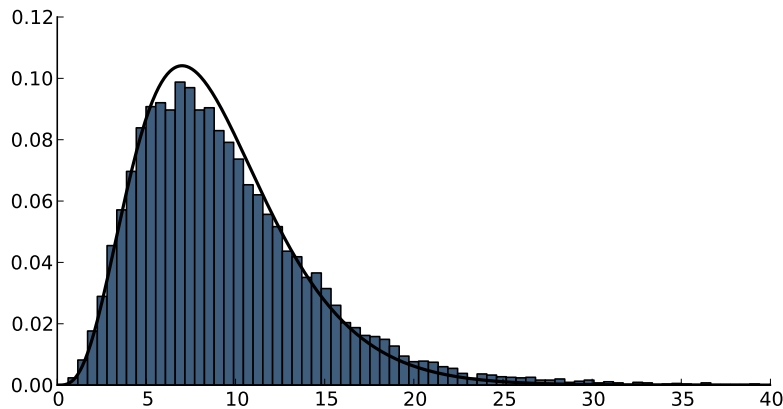


Figure 18. Histogram of $-2 \ln Q$ in the no change region, and theoretical pdf

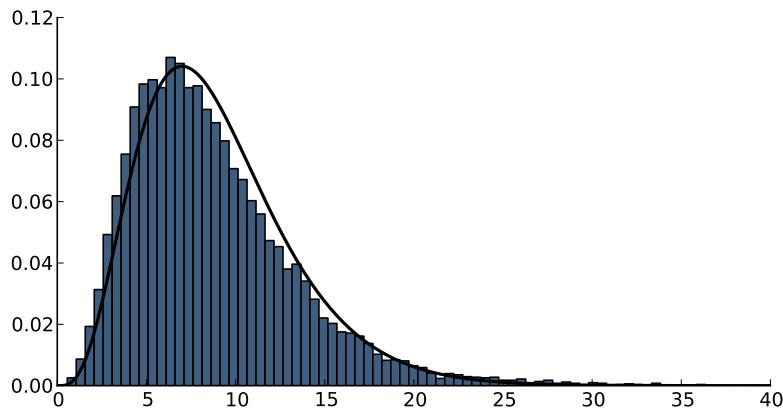


Figure 19. Effect of a lower ENL parameter. Histogram of $-2 \ln Q$ in the no change region, and theoretical pdf with ENL = 12

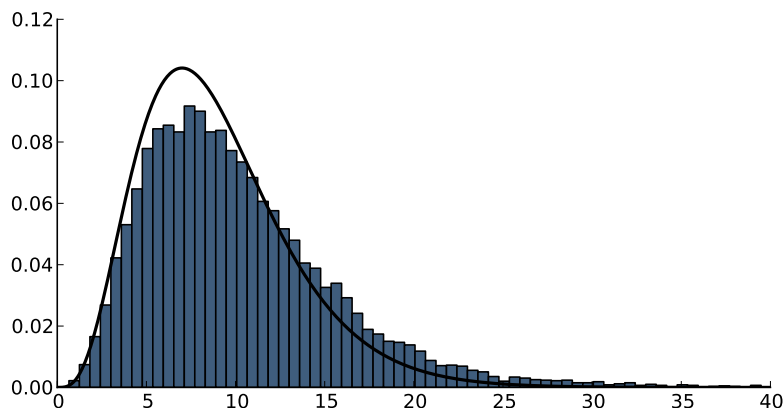


Figure 20. Effect of a higher ENL parameter. Histogram of $-2 \ln Q$ in the no change region, and theoretical pdf with ENL = 14

4.3 Omnibus test statistic

4.3.1 P-values

After having analysed change detection between two radar images, this section presents the results of the Omnibus test statistic. This statistic tests the equality of k covariance matrices:

$$H_j = \Sigma_1 = \Sigma_2 = \dots = \Sigma_k \quad (30)$$

It is given by:

$$Q = \left\{ k^{pk} \frac{\prod_{i=1}^k |\mathbf{X}_i|}{|\mathbf{X}|^k} \right\}^n \quad (31)$$

with $\mathbf{X} = \sum_{i=1}^k \mathbf{X}_i$ and n the equivalent number of looks.

The known distribution of the test statistic under H_0 yield, for each pixel tested, a p-value. It indicates the probability that the time series observations are the result of chance under the hypothesis. After fixing a significance level, for example 1%, the resulting interpretation is that a p-value below 0.01 rejects H_0 and change is detected.

The p-values are computed for each pixel in the image, but an average p-value can be used to characterize an entire area. This is useful with respect to uniform areas like crops. It allow to answer questions such as: Is there any change between March and May in the Forest?

The previous complex Wishart test statistic could be used in pairwise succession to achieve the same result. However it can fail in certain cases, where the change is regular and too slow to be detected between two successive months, but accumulates over the considered time period. This is illustrated by Table 1, where this successive pairwise test with the Wishart test statistic is compared to the Omnibus test statistic. The observed difference is that the Omnibus test can refute H_0 where successive applications of the Wishart test cannot. This is because small changes will go undetected but accumulate over a few months.

	Mar = Apr	Apr = May	May = Jun	Jun = Jul	Jul = Aug	Omnibus
Forest	0.3925	0.6235	0.4913	0.4567	0.4523	0.3494
Rye	0.4249	0.0131	0.3344	0.0242	0.0208	0.0000
Grass	0.2808	0.0638	0.1244	0.4311	0.0000	0.0000

Table 1. P-values comparison using pairwise hypotheses and the Omnibus test.

For example, assuming a threshold of 1% will not detect any change in the Rye field using only pairwise Wishart tests, because all p-values are above 1%. However, the Omnibus test clearly indicates change with a p-value lower than 0.01%.

4.3.2 Images

Change detection images can also be produced with the Omnibus test. Applying the test statistic to the entire image, and taking into account all months of the time series, thresholding at a fixed significance level yields binary images, where white indicates change, and black no-change. Figure 21 shows the result of the procedure. It is a direct extension of the Wishart test statistic (and images shown in Figure 17).

The forest area and lake are clearly visible, especially at lower significance levels. At higher significance levels ($> 1\%$), the change detection images exhibit some noise. This is coherent with the fact that the entire time series of length six is used. With more time points, there are more opportunities for a false positive in a no-change region.

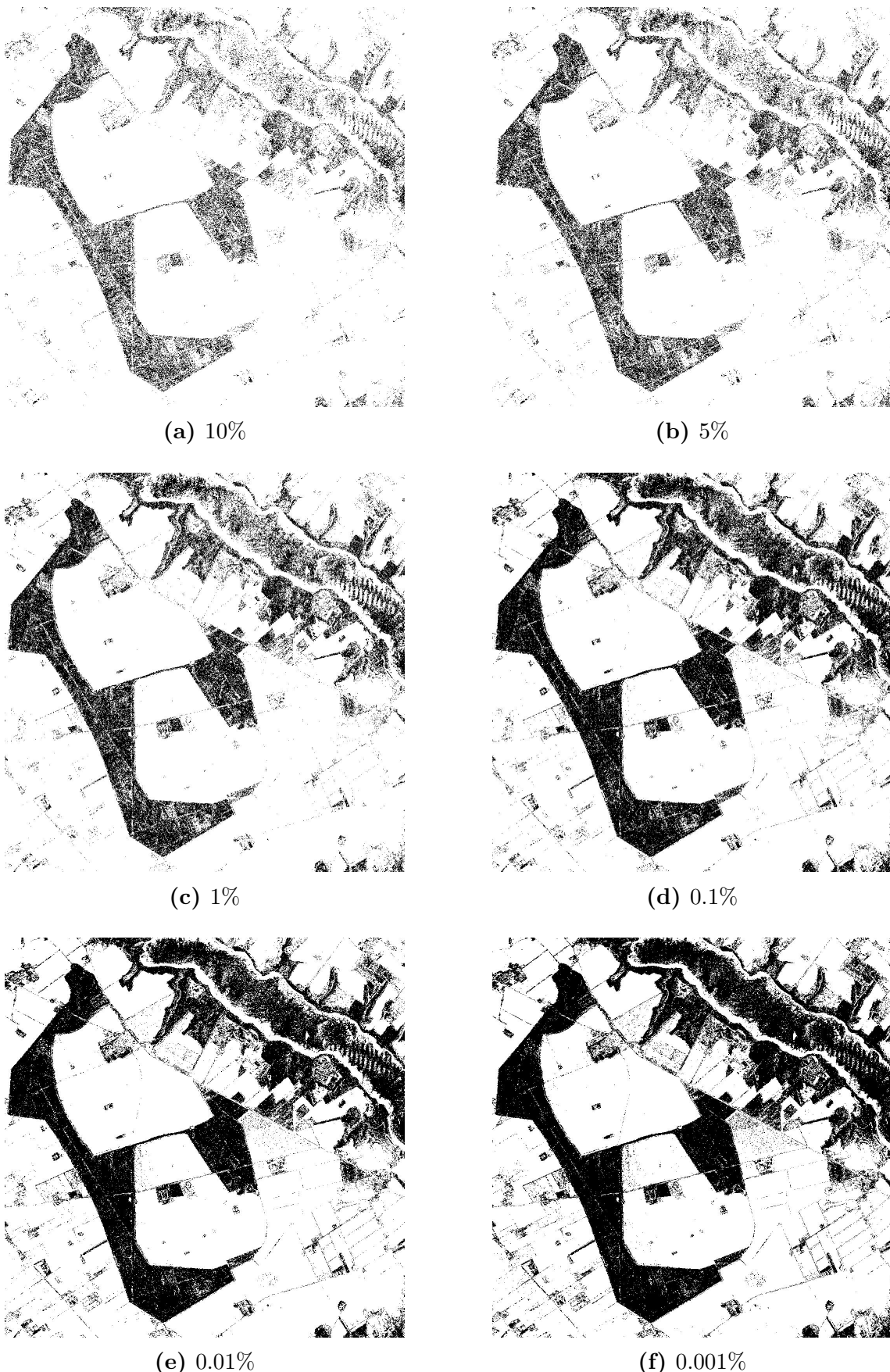


Figure 21. Change detection at different significance levels using the Omnibus test statistic. Black pixels indicate no change in the whole period March to August. White pixels indicate one change or more.

4.4 R_j test statistic

4.4.1 P-values

After change is detected within a time series of images, it is natural to ask: when does change occur? The Omnibus test can be factorized into a product of independent test statistics, as exposed in the Theory section.

Let K_j^l represent the hypothesis:

$$\Sigma_{l+j} = \Sigma_{l+j-1} \quad (32)$$

given that $\Sigma_l = \dots = \Sigma_{l+j-1}$. It is tested with the R_j likelihood ratio:

$$\begin{aligned} \ln R_j = & n \{ p(j \ln j - (j-1) \ln(j-1)) \\ & + (j-1) \ln \left| \sum_{i=l}^{j-1} \mathbf{X}_i \right| + \ln |\mathbf{X}_j| - j \ln \left| \sum_{i=l}^j \mathbf{X}_i \right| \} \end{aligned} \quad (33)$$

Note that in the above equation the sum terms start from l . Together with equation (27) this yields p-values for all hypotheses K_j^l for $l \in [1, k]$ and $j \in [1, k-l]$.

Analysing this result is difficult due to the large amount of p-values. As a first step, they can be organised in a table alongside the marginal hypothesis H_l as shown in Table 2.

Then, the time points of change can be found automatically after choosing a significance level L using the following algorithm:

Algorithm 1. Time points of change.

```

 $j \leftarrow 1$ 
 $l \leftarrow 1$ 
while  $j < k - l + 1$ 
    if  $P(l, j) < L$ 
        Record a change from month  $l+j-1$  to  $l+j$ 
         $l \leftarrow l+j$ 
         $j \leftarrow 1$ 
    else
         $j \leftarrow j + 1$ 

```

where k is the number of elements in the time series and $P(l, j)$ is the p-value associated with the hypothesis K_j^l .

4.4.2 Change visualization

Number of changes

Algorithm 1 yields the exact time points of change for all pixels, and from this can be extracted the total number of changes in the time series. Therefore a simple visualization method is to record this "number of changes" value in an image, and display it with a linear stretch from 0 to $k - 1$. This is done in Figure 22 at different significance levels. It is interesting to compare these images with the previous images obtained using only the Omnibus test (Figure 21). With the number of changes, not only is change detected, the white intensity indicates the number of changes within the entire time period.

Change frequency histograms

Figure 23 shows histograms relative to these grayscale images. They illustrate the distribution of the number of change across the entire image area. As expected, under a higher significance level, less change will be detected because the likelihood ratio fails to reject the hypothesis.

No change periods

The output of Algorithm 1 also contains the months when change occurs. This information can be combined with average p-value over specific subregions of the entire image. By averaging p-values, change can be characterized for these areas, for example agricultural fields. This is done in Figure 24. The continuous blue bands indicate a time period with no change. When change occurs, it is indicated by a discontinuity in the horizontal line, and the p-value of the corresponding K_j^l is displayed as a percentage. This requires the explicit definition of the perimeter of the fields, but allows a compact visualization of the global change pattern over the image. This would be particularly useful with more time points, for example one per week, and for a longer time. With a few years of data, seasonal pattern would be visible with this method.

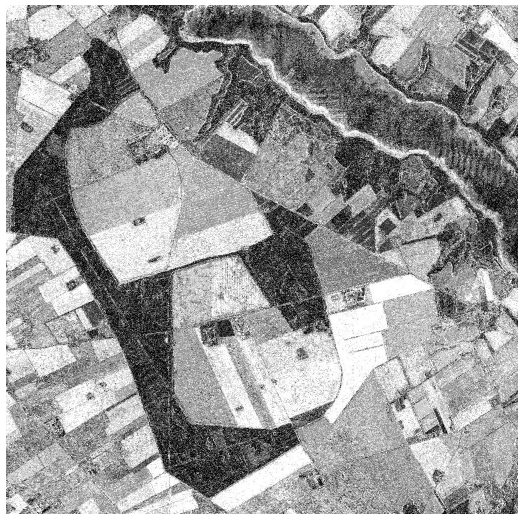
Forest	Mar = ... = Aug	Apr = ... = Aug	May = ... = Aug	Jun = ... = Aug	Jul = Aug
Apr = Mar	0.3925				
May = Apr	0.5469	0.6235			
Jun = May	0.4121	0.4085	0.4913		
Jul = Jun	0.4229	0.4289	0.4629	0.4567	
Aug = Jul	0.4116	0.4099	0.4095	0.4154	0.4523
$P(Q < q)$	0.3494	0.4218	0.4230	0.4108	0.4523

Rye	Mar = ... = Aug	Apr = ... = Aug	May = ... = Aug	Jun = ... = Aug	Jul = Aug
Apr = Mar	0.4249				
May = Apr	0.0026	0.0131			
Jun = May	0.1400	0.2599	0.3344		
Jul = Jun	0.0002	0.0023	0.0237	0.0242	
Aug = Jul	0.1758	0.1292	0.0669	0.0468	0.0208
$P(Q < q)$	0.0000	0.0001	0.0112	0.0080	0.0208

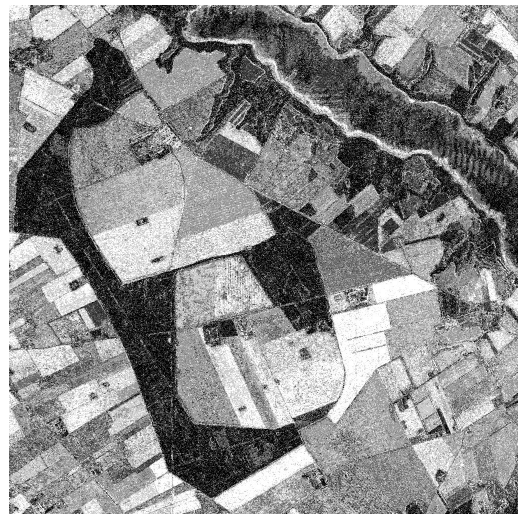
Grass	Mar = ... = Aug	Apr = ... = Aug	May = ... = Aug	Jun = ... = Aug	Jul = Aug
Apr = Mar	0.2808				
May = Apr	0.0112	0.0638			
Jun = May	0.0056	0.0319	0.1244		
Jul = Jun	0.1094	0.2386	0.3879	0.4311	
Aug = Jul	0.0000	0.0000	0.0000	0.0000	0.0000
$P(Q < q)$	0.0000	0.0000	0.0000	0.0000	0.0000

W. Wheat	Mar = ... = Aug	Apr = ... = Aug	May = ... = Aug	Jun = ... = Aug	Jul = Aug
Apr = Mar	0.3756				
May = Apr	0.0013	0.0051			
Jun = May	0.0270	0.0478	0.0872		
Jul = Jun	0.0030	0.0102	0.0547	0.1492	
Aug = Jul	0.0924	0.0903	0.0704	0.0392	0.0338
$P(Q < q)$	0.0000	0.0001	0.0119	0.0272	0.0338

Table 2. Tables of p-values for the Forest, Rye, Grass and Winter Wheat regions.



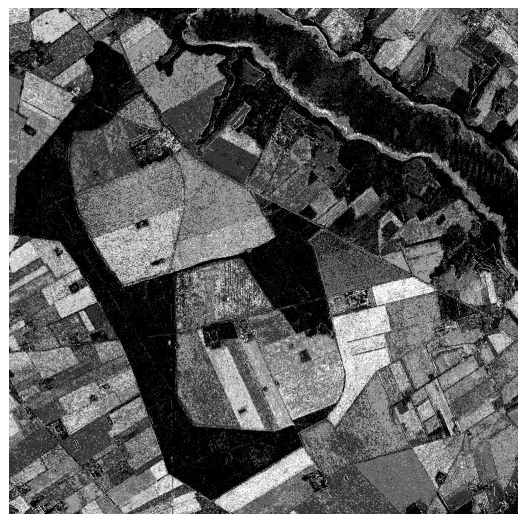
(a) 10%



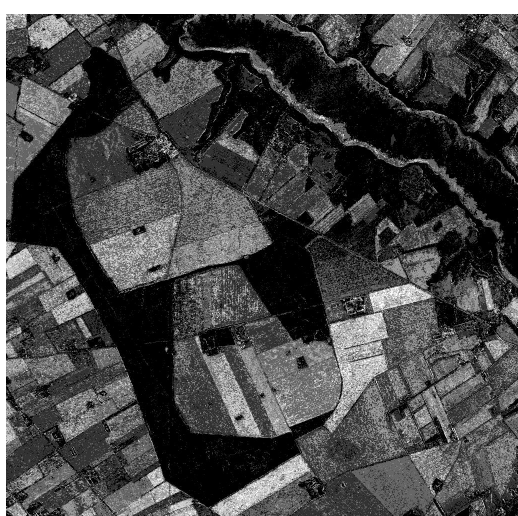
(b) 5%



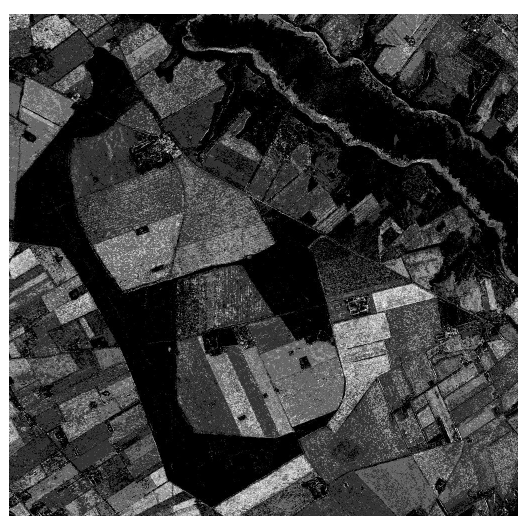
(c) 1%



(d) 0.1%



(e) 0.01%



(f) 0.001%

Figure 22. Images of the number of changes using the R_j test statistic at different significance levels. White intensity is proportional to the number of changes between March and August.

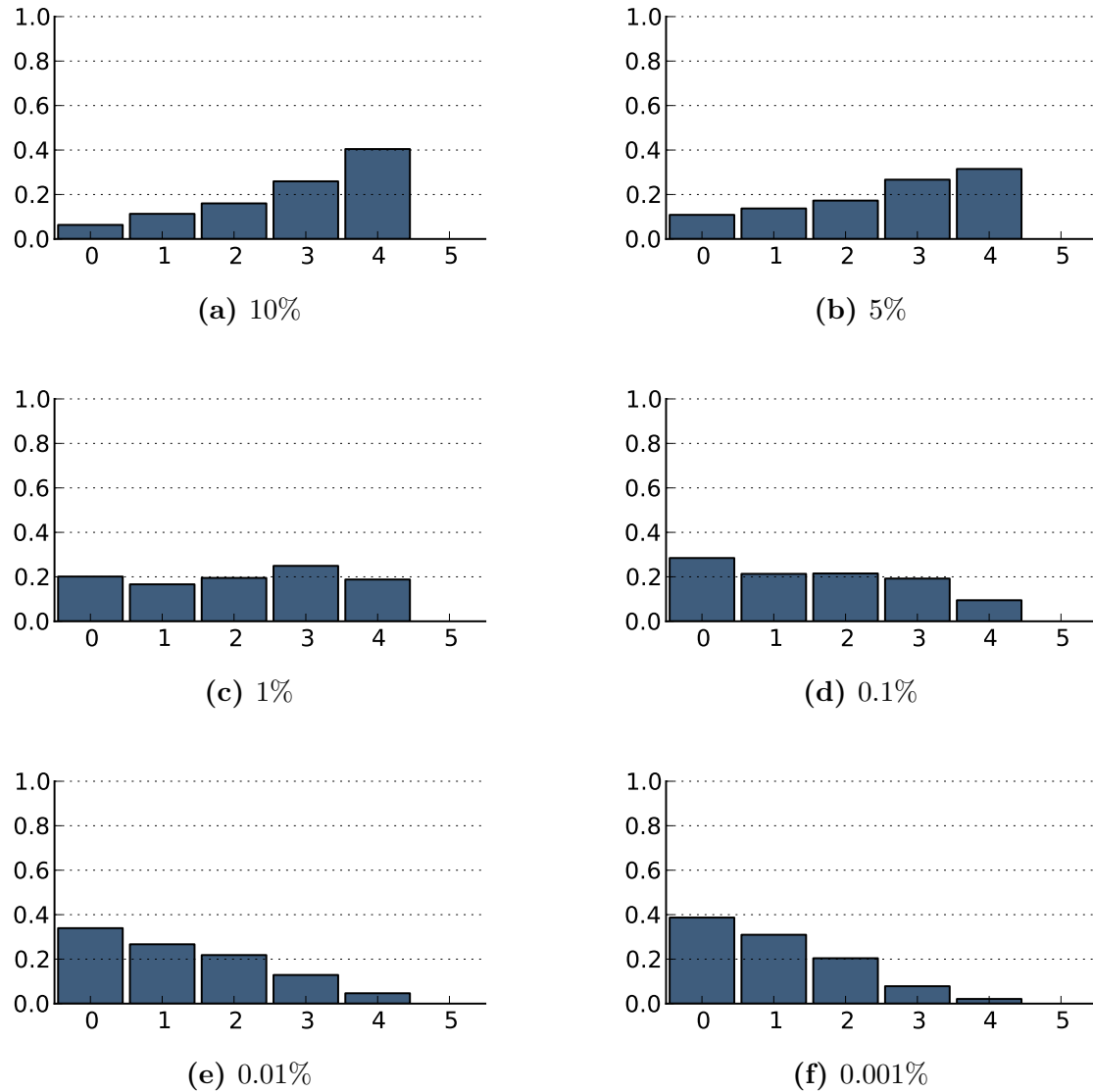


Figure 23. Histograms of the number of changes detected over the entire image at different significance levels with the R_j test statistic.

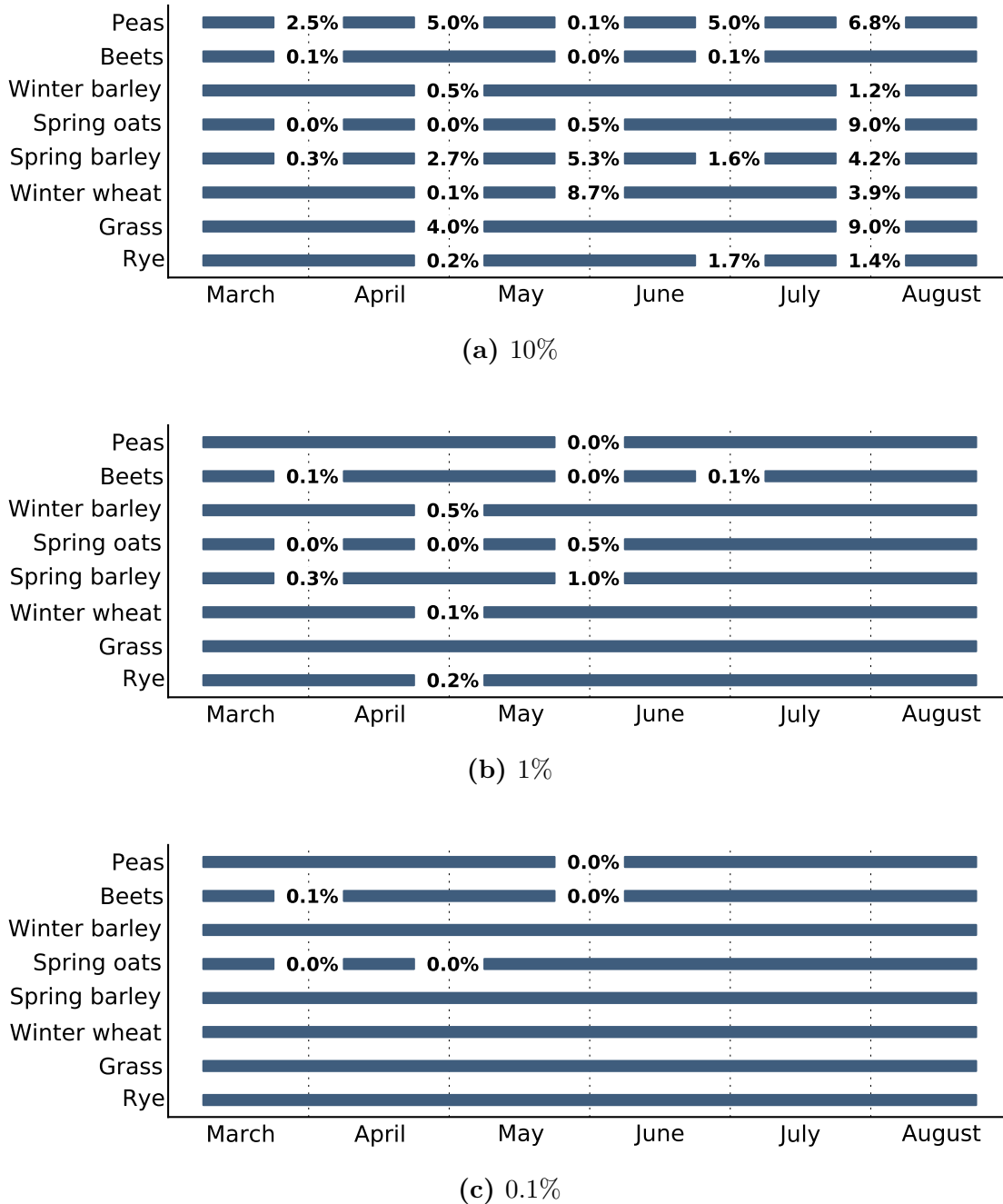


Figure 24. Change patterns of agricultural fields in the image.

5 Implementation

This section is a brief overview of the tools and methods used for implementing the experimental part of this project.

5.1 Tools

Python

Implementation of the test statistics, reading the Foulum data set, processing the images and producing the plots and images was made with the Python programming language.

Scipy

Scipy [5] is a library in addition of Python for scientific computing. It was used for matrix algebra and computing probability density functions and quantiles.

Plotting

The matplotlib [4] Python library was used for producing the images, graphs and figures in this report.

5.2 Efficiency considerations

Memory usage

In its present state, the Python implementation is not optimized for memory usage. The entire data set for all six months of images is less than 230 MB. This fits comfortably within computer memory, and therefore a better implementation with respect to memory was not needed for this project. However, all the procedures presented can be implemented with $\mathcal{O}(1)$ memory usage, by processing the SAR data in fixed size chunks. This would be most efficient when combined with a chunk size equal to the size of a system's CPU cache, to minimize I/O operations.

Determinant

The covariance matrix is Hermitian, so its determinant is real. It is computed directly from its elements:

$$\begin{vmatrix} a & d & e \\ d^* & b & f \\ e^* & f^* & c \end{vmatrix} = abc + dfe^* + ed^*f^* - ebe^* - dd^*c - aff^*$$

The elements d^* , e^* and f^* correspond to $S_{hv}S_{hh}^*$, $S_{vv}S_{hh}^*$ and $S_{vv}S_{hv}^*$. They are not stored in memory but computed from their complex conjugate when they are

needed. This divides the memory requirement by two, without significantly reducing speed efficiency since complex conjugating is trivial.

In the special case of azimuthal symmetry, the determinant simplifies to:

$$\begin{vmatrix} a & d & 0 \\ d^* & b & 0 \\ 0 & 0 & c \end{vmatrix} = c(ab - dd^*)$$

Finally, when considering only the diagonal elements the determinant is simply the product: $S_{hh}S_{hh}^* \times S_{hv}S_{hv}^* \times S_{vv}S_{vv}^*$.

Speed

Despite the fact that Python is an interpreted programming language, processing time of this project's implementation is very reasonable. The Scipy library uses vectorized operation over arrays to avoid repetitive *for* loops. The overhead of Python's interpreter is therefore minimized.

6 Conclusion

This project investigated methods of change detection in polarimetric SAR images. In the first part only two time points were considered. With the test statistic for the equality of two complex Wishart distributed covariance matrices, change detection is effectively achieved. The results are quantifiable with p-values and images can be produced that identify the intensity of the change. For example, the difference between a non changing area (the forest) and a grass field is clear. The theoretical distribution of the test statistic was also investigated and verified experimentally.

The second part of this project analysed extensions of the complex Wishart test statistic to an arbitrary number of time points. A generalization of the likelihood ratio test, called the Omnibus test, allows a complete time series of image to be considered. This test considers the hypothesis of all parameters being equal at all time points. When this hypothesis is rejected, a factorization of the likelihood ratio into a product where each element tests a simpler hypothesis, together with a simple algorithm, allow the determination of the precise time points at which change occurs.

The efficient interpretation of the results provided by this test is a challenge. P-values provide a lot of unstructured information. This project implemented a few of the visualization possibilities:

- **Change map** (Figure 21). A thematic map where black pixels indicate the absence of change in the entire time period, and white pixels the presence of at least one change.
- **Number of changes map** (Figure 22). A direct extension of the previous change map where instead of a binary value, the intensity indicate the number of changes that occurred in the entire time period.
- **No change periods** (Figure 24). A compact representation of the change patterns of all agricultural fields visible in the image.

The opportunity of change detection in polarimetric SAR data is very valuable for all monitoring applications, including agriculture, surveillance, earth system science and others. Interpretation of the results can be a challenge, but compact and rigorous visualizations can be set up to greatly facilitate usage of advanced radar systems.

Future work

The scope of this project was limited in time, and there are many interesting possibilities for future research in this domain.

- In section 4.2.1, an approximation was used for estimating the quantiles of the distribution of $P\{-2\rho \ln Q\}$. It would be interesting to use an iterative method to better approximate the true distribution, or extract quantiles from the experimental distribution and see if there are any effects on the result.
- More visualization of the result of the R_j statistic can be explored. In particular, with more time points of data it would be interesting to try to detect seasonality in the changes.
- As discussed in section 5.2, a constant memory implementation would allow an arbitrary large amount of data to be processed, with the only impact being processing time.

References

- [1] Knut Conradsen, Allan Aasbjerg Nielsen, and Henning Skriver. “A test statistic for Equality of Several Complex Variance-Covariance Matrices Applied to Change Detection in Polarimetric SAR Data”. In: *IEEE Transactions on Geoscience and Remote Sensing, submitted to* (2015).
- [2] Knut Conradsen, Allan Aasbjerg Nielsen, Jesper Schou, and Henning Skriver. “A test statistic in the complex Wishart distribution and its application to change detection in polarimetric SAR data”. In: *Geoscience and Remote Sensing, IEEE Transactions on* 41.1 (2003), pp. 4–19.
- [3] Knut Conradsen, Allan Aasbjerg Nielsen, and Henning Skriver. “Determining the Points of Change in Time Series of Polarimetric SAR Data”. In: *IEEE Transactions on Geoscience and Remote Sensing, submitted to* (2015).
- [4] J. D. Hunter. “Matplotlib: A 2D graphics environment”. In: *Computing In Science & Engineering* 9.3 (2007), pp. 90–95.
- [5] Eric Jones, Travis Oliphant, Pearu Peterson, et al. *SciPy: Open source scientific tools for Python*. [Online; accessed 2015-01-30]. 2001–. URL: <http://www.scipy.org/>.